

## Effects of cobalt content on martensitic transformation and shape memory effect in Fe-Mn-Si-Cr-Ni alloys

B. Jiang, K. Xu, X. Qi and W. Zhou

*Key Laboratory for High Temperature Materials & Tests of Ministry of Education, Shanghai, Jiaotong University, Shanghai 200030, China*

**Abstract.** The effects of cobalt content on the stacking fault probability ( $P_{sf}$ ) determined by means of X-ray diffraction profile analysis and associated with the starting temperature of  $\gamma \rightarrow \epsilon$  transformation ( $M_s$ ) and the strain-hardening exponent ( $n$ ) etc, have been investigated in Fe-Mn-Si-Cr-Ni based alloys with four different contents of Co from 0.39% to 3.93%(wt). The results show that  $M_s$  and  $n$  increase with increasing Co content which is related to the increase of the stacking fault probability owing to the addition of cobalt. Addition of proper content of cobalt in Fe-Mn-Si-Cr-Ni alloy can improve its SME.

### 1 INTRODUCTION

Fe-Mn-Si-Cr-Ni based shape memory alloys have been studied intensely [1] because of their good corrosion resistance and better cold-deformation property than Fe-Mn-Si based alloys. For fcc ( $\gamma$ )  $\rightarrow$  hcp ( $\epsilon$ ) martensite transformation the stacking faults play an important effect on the phase transformation and SME. As is known, Si and Co decrease stacking fault energy (SFE)[2], moreover, raise  $M_s$ . The effects of Si on SME have been widely investigated [2,3,4,5]. However, the effect of cobalt on SFE and SME in Fe based SMAs is not yet been systematically studied.

### 2. EXPERIMENTAL PROCEDURE

Four alloys were prepared by vacuum induction melting using high purity iron, manganese, silicon, chromium, nickel, and cobalt. The composition of specimens is shown in Table 1.

Table 1 Composition of Alloys, wt%

Alloy	Co	Mn	Si	Cr	Ni	Fe
No.1	0.39	14.07	6.14	12.12	5.06	balance
No.2	0.98	13.31	6.81	13.32	4.98	balance
No.3	2.77	13.84	6.49	13.12	5.14	balance
No.4	3.93	13.78	6.58	13.29	4.95	balance

After homogenization at 1373K for 8hr, the ingots were forged, hot-rolled and cold-drawn to wire with a diameter of 1mm, from which samples for tensile test, optical microscope observation and X-ray analysis were cut. The samples were austenitized at 1223K for 40 min then cooled to 973k, followed by water quenching. After grinding and chemical polishing, the tensile samples with length of 140 mm were

extended using Shimadzu Test Machine at room temperature. After unloading the extended samples were heated up to 873K for reverse transformation. The thermo-mechanical training was carried out for four cycles. The degree of shape recovery and the recovery strain were determined from the change in gauge length of a sample at room temperature using the definition  $\eta(\%) = (L_1 - L_2)/(L_1 - L_0) \times 100$ , and  $\varepsilon_r(\%) = (L_1 - L_2)/L_0 \times 100$  respectively, where  $L_0$ ,  $L_1$  and  $L_2$  are the gauge length before and after tension, as well as after recovery, respectively. The 0.2% proof stress of the alloys was measured from the stress-strain curve. The strain-hardening exponent  $n$  was calculated according to the formula  $\sigma = K \varepsilon^n$  from the true stress-strain curve. The transformation temperature was measured by electrical resistance test.

The stacking fault probability  $P_{sf}$  was measured by XRD profile analysis method [6,7]. In this work the Gaussian function  $y = a \exp(-\beta x^2)$  was adopted to describe the measured diffraction profile. According to Scherrer's equation, a mean effective crystallite (domain) size  $D_{eff}$  involving the effect of true coherent domain size  $D_{sb}$  and the probability of stacking fault  $P_{sf}$ , can be established by following function

$$D_{eff} = \frac{\lambda}{\beta \cos \theta_{hkl}} \quad (1)$$

where  $\lambda = 0.15406\text{nm}$ , is the wavelength of Cu  $K_{\alpha 1}$ , and  $\theta_{hkl}$  is the diffraction angle.  $\beta$  is integrated width of diffraction peak. Applying effective crystallite size calculated from (111) and (200) diffraction peaks of the  $\gamma$ -phase, we can obtain  $P_{sf}$  by following equations:

$$\left( \frac{1}{D_{eff}} \right)_{111} = \frac{1}{D_{sb}} + \frac{P_{sf}}{a_0} \cdot \frac{\sqrt{3}}{4} \quad (2)$$

$$\left( \frac{1}{D_{eff}} \right)_{200} = \frac{1}{D_{sb}} + \frac{P_{sf}}{a_0} \quad (3)$$

where  $a_0$  being the lattice parameter of the  $\gamma$ -phase[5].

### 3.RESULTS

The determined  $M_s$  temperatures and stacking fault probabilities  $P_{sf}$  of four alloys are listed in Table 2.

Table 2. Effects of Co contents on  $M_s$ ,  $P_{sf}$ ,  $n$ ,  $\sigma_{0.2}$

Alloy	Co (wt%)	$M_s$ (K)	$P_{sf} (\times 10^{-3})$	$n$	$\sigma_{0.2}$ (MPa)
No.1	0.39	286.5	2.24	0.1368	436.0
No.2	0.98	288.5	2.51	0.1410	392.2
No.3	2.77	290.5	3.11	0.1458	424.4
No.4	3.93	294.3	4.99	0.1474	380.7

From Table 2 we can see that  $M_s$  and  $P_{sf}$  increase with the increase in cobalt contents. The XRD spectrum at room temperature for the four tested alloys are shown in Fig.1. It is clearly shown that except austenite structure, the intensities of diffraction beam of  $\varepsilon$  martensite increases with increasing cobalt content.

The shape recovery rate  $\eta$  vs. cycle numbers are shown in Fig.2. It shows that  $\eta$  increases with training numbers for all alloys, however, the alloy No.3 exhibits the best shape memory effect.

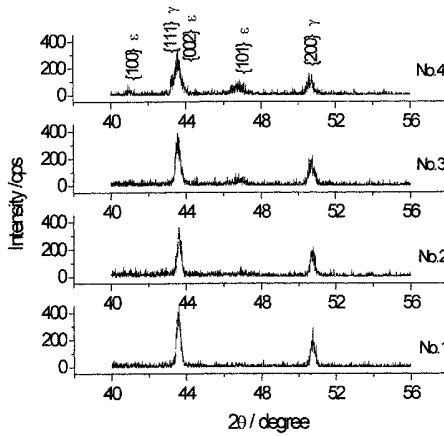


Fig.1. X-ray diffraction spectrum for the four alloys  
The Co contents increase from No.1 to No.4

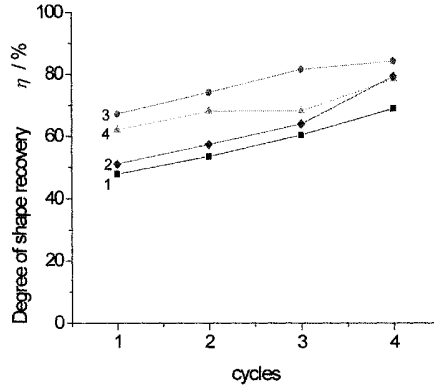


Fig.2. Degree of shape recovery  $\eta$  vs. cycles  
in four alloys

#### 4. DISCUSSION

From the results of Table.2 and Fig.1 we can see that the  $M_S$  point increase with cobalt content, which is consistent with most ferrous alloys. For  $\gamma$  (fcc)  $\rightarrow$   $\epsilon$  (hcp) phase transformation in Fe-Mn-Si based SMAs, the nucleation of  $\epsilon$ -martensite is mainly dependent on the overlapping of stacking faults [8]. With lower stacking fault energy (SFE) of austenite, the chemical driving force needed for the formation of martensite becomes lower, thus  $M_S$  temperature rise. However, in those alloys, their SFE are relatively lower, it is difficult to determine that by TEM or other experimental method. So we measure the stacking fault probability  $P_{sf}$  by XRD profile analysis. The  $P_{sf}$  is known to be inversely proportional to SFE, i.e.  $SFE \propto 1/P_{sf}$  [7,8]. When we put  $M_S$  versus  $1/P_{sf}$  for alloys with different Co contents, a linear relationship is well established as shown in Fig.3. From linear regression of the data for the four alloys we got the equation,  $M_S(K)=300.5-0.031/P_{sf}$ .

Stacking faults do not only affect  $\epsilon$ -martensitic transformation related to the motion of the Shockley partial dislocation, but also work on the deformation behavior related to the movement of a perfect dislocation in the  $\gamma$  phase. In the present work the strain-hardening exponent  $n$  estimated from true stress-strain curves increased monotonically with increasing cobalt content shown as Fig.4.

Once the applied stress exceeds the yield stress of  $\gamma$ -phase, the perfect dislocations start to move. In alloys with a low stacking fault energy, a perfect dislocation can easily decompose into two partial dislocations with a stacking fault ribbon, forming an extended dislocation. When two extended dislocations on the conjugate slip planes intersect each other, extended jogs and Cottrell-Lomer locks are formed and become barriers to the further motion of dislocations, leading to the increase in strain hardening. The higher  $P_{sf}$  the alloys have, the wider the stacking fault ribbons are and consequently the more difficult the cross-slip is, causing the increase in the strain-hardening exponent [7].

Fig.2 shows that shape recovery rate  $\eta$  firstly increases and then slightly decreases (e.g.No.4) with the increase of cobalt content, and the maximum of  $\eta$  is obtained in No.3 alloy.

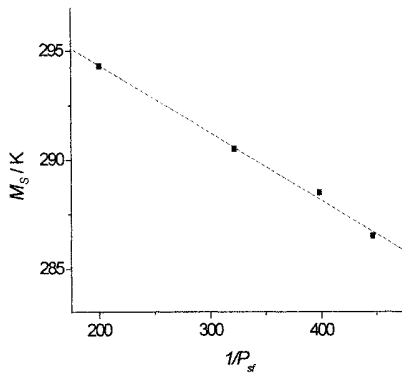
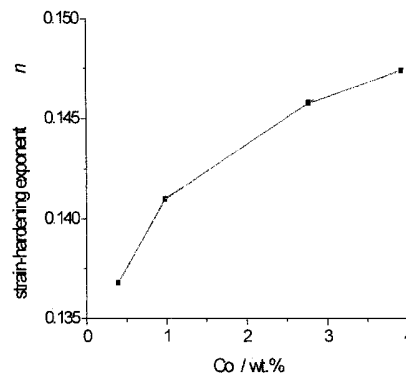
Fig.3. The relationship between  $1/P_{sf}$  and  $M_s$ 

Fig.4. Variation of strain hardening exponent versus Co contents

It can be explained that cobalt enhances the  $P_{sf}$  and  $n$ , that benefit to the motion of partial dislocations whereas retard the movement of perfect dislocations. However, it has no contribution to the strength of parent phase [4], and even lowers the strength of the alloy as adding much higher Co content for example alloy No.4. The SME of alloys is the synthesis results of these factors.

## 5. CONCLUSIONS

1. The effect of cobalt content in Fe-Mn-Si-Cr-Ni SMA is mainly enhancing the stacking fault probability  $P_{sf}$  lowering the SFE, so that increasing martensitic transformation temperature  $M_s$  and strain-hardening exponent  $n$ .
2. A linear relationship between  $M_s$  and  $1/P_{sf}$  in this kind of alloy is established as  

$$M_s(K) = 300.5 - 0.031/P_{sf}$$
3. By adding optimal amount of cobalt to Fe-Mn-Si-Cr-Ni alloys, SME may be improved.

## References

- [1] Miyazaki S., Otsuka K., ISIJ. Inter., 1989, 29:353.
- [2] Murakami M., Otsuka H., Suzuki G., Matsuda S., Proc. ICOMAT-86, Jpn. Inst. Metals, 1987, 985.
- [3] Ghosh G., Vanderveken Y., Van Humbeeck J., Chandrasekaran. M., Delaey L., Vanmoorlegheem W., Proc. MRS Inter. Meeting on Advanced Materials, vol. 9, Ed. Doyama M. et al., MRS., Pittsburgh, 1989, 457.
- [4] Maki T., in Shape Memory Materials, Ed. Otsuka K., Wayman C. M., Cambridge University Press., 1998, Chapter 5.
- [5] Tsuzaki, Ikegami M., Tomota Y., Kurokawa Y., Nakagawara W., Maki T., Mater. Trans. JIM., 1992, 33:263
- [6] Warren, B. E., X-ray Diffraction Addison-Wesley, Reading, Ma., 1969, pp. 275-294.
- [7] B.H.Jiang, X.Qi, S.X.Yang, W.M.Zhou, and T.Y.Hsu (Xu Zuyao), Acta Mater. 46, 1998, pp.501-510.
- [8] Reed, R. P. and Schramm, R. E., J. appl. Phys., 1974, 45, 4705.